Publications of the Astronomical Society of the Pacific
104: 958–975, 1992 October

Astrometric Performance Characteristics of the *Hubble Space Telescope* Fine Guidance Sensors[1]

G. F. BENEDICT, E. NELAN, D. STORY, B. MCARTHUR, AND A. L. WHIPPLE

McDonald Observatory, University of Texas, Austin, Texas 78712
Electronic mail: fritz@dorrit.as.utexas.edu, nelan@scivax.stsci.edu, story@scivax.stsci.edu, mca@astro.as.utexas.edu, alw@astro.as.utexas.edu

W. H. JEFFERYS

Department of Astronomy, University of Texas, Austin, Texas 78712
Electronic mail: bill@bessel.as.utexas.edu

W. VAN ALTENA

Department of Astronomy, Yale University, New Haven, Connecticut 06511
Electronic mail: vanalten@yalastro.bitnet

P. D. HEMENWAY AND P. J. SHELUS

McDonald Observatory, University of Texas, Austin, Texas 78712
Electronic mail: paul@astro.as.utexas.edu, pjs@astro.as.utexas.edu

O. G. FRANZ

Lowell Observatory, Mars Hill Road, 1400 West, Flagstaff, Arizona 86001
Electronic mail: ogf@lowell.edu

A. BRADLEY

Allied Signal Aerospace Company, Bendix Guidance Systems Division,
P. O. Box 91, Annapolis Junction, Maryland 20701
Electronic mail: bradley@ap5.gov

L. W. FREDRICK

Department of Astronomy, University of Virginia, Charlottesville, Virginia 22903
Electronic mail: lwf@virginia.bitnet

R. L. DUNCOMBE

Aerospace Engineering, University of Texas, Austin, Texas 78712
Electronic mail: aoug065@emx.utexas.edu

Received 1992 May 11; accepted 1992 June 23

ABSTRACT. Each of the three Fine Guidance Sensors for the *Hubble Space Telescope* constitutes a sixth science instrument to be used for astrometry. We detail the tests and results used in choosing one of the three sensors to be the prime astrometer. The Astrometry Science Team has chosen Fine Guidance Sensor (FGS) 3. FGS 3 produces position measurements on a star with $V=17$ with a per-axis precision of 0.003 arcsec. The interferometer response function should permit double-star astrometry at least down to $V=16$ for the central region of FGS 3. In a 10-h test of the stability of POS-mode astrometric measurements made in FGS 3, we found no scale or orientation variations greater than two parts in 10^5. During this same time period, we found no statistically significant systematic guide-star radial separation changes. Spacecraft jitter is found to be the prime determinant of astrometry success or failure.

1. INTRODUCTION

Will the *Hubble Space Telescope (HST)* have astrometric utility? As described in Jefferys et al. (1985), *HST* has great astrometric potential. The by now well-known problems afflicting *HST* have certainly reduced its astrometric capabilities. However, these problems have not rendered *HST* astrometrically unusable. In support of this assertion we offer results from some initial testing.

The Orbital Verification phase for *HST* astrometry was designed to test the engineering aspects of Fine Guidance Sensor astrometry. FGS astrometry measurements with *HST* fall into two broad categories: position mode (POS) and transfer scan (TRANS) mode. A detailed discussion of these modes and the required post-observation data processing can be found in Bradley et al. (1991). Our original

[1]Based on observations with the NASA/ESA *Hubble Space Telescope*, obtained at the Space Telescope Science Institute, which is operated by the Association of Universities for Research in Astronomy, Inc., under NASA Contract No. NAS5-26555.

plan consisted of many tests of each of the three FGS units to determine which was best suited for astrometry. During Orbital Verification we specifically addressed these crucial questions: Could we acquire stars in POS-mode fine lock and obtain positions of astrometric significance? On how faint a star could we obtain such measurements? Would the FGS interferometer response function permit detection of faint binaries? What effect would a changing thermal environment have on POS-mode astrometry? Other issues included verification of filter type within each filter wheel and exploration of the effects of user selectable FGS operating parameters.

The discovery of spherical aberration in the primary mirror (Burrows et al. 1991) and the subsequent discovery of internal misalignments within each FGS (Benedict et al. 1991) have resulted in serious delays to our astrometric program. The original Orbital Verification tests were to have been completed two months after launch. Two years after launch we approach the conclusion of Astrometry Orbital Verification. We have directed much of our effort to finding a secondary mirror position which would result in at least one FGS being usable as an astrometer. We have succeeded. However, the combination of the aforementioned internal misalignments and the final secondary mirror position renders FGS 2 virtually unusable for astrometry, and only marginally usable for guiding. This paper presents the results of our Orbital Verification testing, documenting why we choose FGS 3 as the prime astrometer. Given the poor performance of FGS 2 at the final collimation secondary mirror position (determined by a "Nine Points of Light" test described in Sec. 3 below), we decided to further test only FGS 3 and FGS 1.

We shall report results from three different Orbital Verification tests. These include Astrometry Verification, a Nine Points of Light test (see Benedict et al. 1991 for a test description), and a Short-Term Thermal Stability test. These results are organized as follows. We first discuss the verification of filter position within FGS 1 and FGS 3. Next we present test results concerning TRANS mode astrometry, i.e., that done by analyzing the response function of the FGS interferometer obtained by moving the FGS instantaneous field of view across a target. Then we detail results of POS-mode tests. In this mode the FGS electronics reports a stream of positions as the instrument continually seeks the null, or zero-point crossing of the transfer function. One major concern for TRANS and POS mode was the limiting magnitude. We were also concerned with determining correct instrumental gains. These are the uplinked, observation- , and FGS-dependent K factors used to derive the Fine Error Signal from the interferometer response function (Bradley et al. 1991). Finally we assess the effects of a changing (but fairly typical) thermal environment on POS-mode astrometry.

The stars observed during the Astrometry Verification test are listed in Table 1. They are all located near NGC 188. The faint stars are from a list of photoelectric observations from Sandage (1962). The brighter stars are listed in Upgren et al. 1972. All VA star positions are from a special guiding catalog produced by van Altena et al. (1992) for the Space Telescope Science Institute. The Sandage star positions were measured on a Palomar Observatory Sky Survey glass copy plate, using the McDonald Observatory PDS astrometry system (Benedict and Shelus 1978). Table 2 provides positions and photographic magnitudes (from the Guide Star Selection System catalog, Lasker et al. 1990) for the stars used in the thermal test.

TABLE 1
Target Stars in NGC 188

Star	ID	VA ID	RA (2000)	DEC	V	B-V
1	UPGREN-69	998	0h 42m 42.0952s	85° 14' 14.366"	9.58	0.50
2	UPGREN-112	1448	0 45 53.4167	85 19 55.579	10.84	1.28
3	UPGREN-111	1357	0 45 51.1405	85 18 8.406	12.41	1.34
4	UPGREN-108	1376	0 45 44.0385	85 18 37.334	15.03	0.69
5	SANDAGE-I117		0 45 55.04	85 14 46.1	17.40	0.92
6	SANDAGE-I118		0 46 16.87	85 14 56.5	17.02	1.06
7	SANDAGE-I166		0 48 51.32	85 14 42.3	18.03	1.26
8	UPGREN-138	1120	0 47 3.8981	85 15 27.718	14.28	0.88
9	SANDAGE-I95		0 48 20.82	85 13 1.5	16.06	0.72

Positions of VA stars ± 0.005 arcsec
Positions of Sandage stars ± 0.3 arcsec
Magnitudes ± 0.1

2. FILTER POSITION VERIFICATION

Are the filters in each FGS unit in their proper positions? In the notation of the FGS Instrument Handbook (Taff 1991) we have F583W (a piece of glass in the filter wheel, also called the clear filter), PUPIL (a roughly 2/3 aperture stop in the filter wheel, again, containing a piece of glass to equalize the optical paths), F5ND (a neutral density 5 filter to be used in observing bright stars), F550W, and F605W. Potential uses of these filters are discussed in Bradley et al. (1991). The filter targets are stars 2 and 4 in Table 1. Due to terminator-induced disturbances which caused a loss of lock, we have no fine-lock data for the filter tests. However, subsequent to each jolt, the positional drift was usually small, so the PMT counts in those cases should be reasonably reliable. However, this was not the case for the F583W observation of Upgren-69 with FGS 1. Due to a disturbance and resulting loss of lock, the star moved completely out of the aperture. Table 3 lists the raw instrumental magnitudes $[-2.5 \log(\text{intensity})]$ for FGS 1 and FGS 3 through the various filters.

We verified F583W by showing that it produces the highest throughput on any star. This can be seen in line 1 of Table 3. We verified PUPIL by comparing these measures with those from F583W. There should be a 0.75 mag difference between the two. This was found to be the case for two out of three of the comparisons (line 7, Table 3). The bottom line of this table verified that the F5ND filter

TABLE 2
Stars Used for Thermal Stability Test

ID	RA (2000)	DEC	V
1	22h 21m 41.6s	- 8° 53' 13.6"	11.57
3	22 21 33.3	- 8 54 5.5	13.03
4	22 21 36.85	- 8 54 34.1	14.27

Positions ± 0.5 arcsec
Magnitudes ± 0.8

TABLE 3
Filter Position Verification

		FGS Star	FGS 3 U 69	FGS 3 U 111	FGS 1 U 69	FGS 1 U 111
			raw magnitudes			
	Filter					
1	F583W (clear)		-10.17	-7.52		-7.32
2	F5ND (ND 5)		-5.15	-2.60	-5.50	-3.08
3	F605W		-9.92	-7.27	-8.46	-6.02
4	PUPIL (2/3 aperture)		-9.62	-6.77	-9.37	-6.55
5	F550W		-9.12	-6.32	-8.91	-6.11
			raw magnitude differences			
6	F605W-F550W		-0.81	-0.95	0.45	0.09
7	PUPIL-F583W		0.54	0.76		0.77
8	F5ND-F583W		5.01	4.92		4.24

is properly installed. Compared with F583W (clear), these observations should be 5 mag fainter.

We verify the positions of F550W and F605W by comparing the throughput for a red (Upgren-111) and a blue (Upgren-69) star. The ratio F605W/F550W should be higher for the redder star. Thus, the instrumental color indices (F550W–F605W) (line 6, Table 3) should be smaller for the bluer star. In each case, they are.

As a very low-order test of the performance of FGS 3 we determine that the noise has a Poisson distribution by plotting (Fig. 1), the square root of the average FGS 3 photomultiplier signal against the standard deviation of the signal. This is the average of the sum of the four photomultiplier channels, two on each interferometer axis.

Figures 2(a) (FGS 1) and 2(b) (FGS 3) show the instrumental magnitudes plotted against ground-based values of V for the F583W and F550W data acquired during the entire Astrometry Verification test. The relationships are linear, as expected. It seems likely that the $V=18$ star (No. 8, Table 1) is closer to $V=17.6$. Even though we had very large measurement errors in position, on the order of 0.1 arcsec, it seems clear from the average PMT counts (Fig. 2) that we did acquire Sandage-I117 ($V=17.4$) and Sandage-I166 ($V\approx17.6$) in a photometric, if not astrometric, sense.

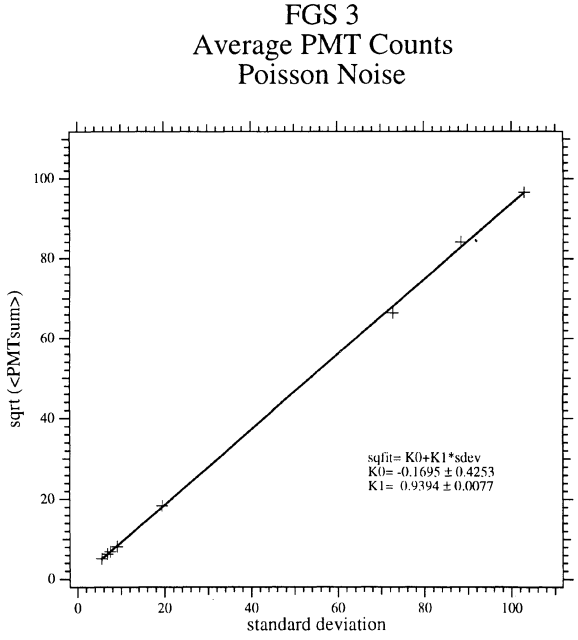

FIG. 1—We compare the square root of the average photomultiplier (PMT) counts against the calculated standard deviation of these counts. The relationship is linear, implying that $\sigma \propto \sqrt{\text{count}}$. Hence, the noise has a Poisson distribution.

Finally, we can assess the absolute sensitivity of FGS 3 relative to FGS 1. For the same stars observed through the same F550W filter, FGS 3 appears to be 0.28 mag more sensitive than FGS 1. In other words, for the same measured instrumental magnitude, we can observe a star 0.28 mag fainter with FGS 3 than with FGS 1. This is the difference between the K0 coefficients (listed in the plot legends of Fig. 2) derived for the F550W comparisons.

3. TRANS MODE

The shape of the FGS interferometer response function (also referred to as the transfer function, or S curve) critically determines astrometric efficacy in both TRANS and POS mode. An S curve is generated by scanning the 5-arcsec-square FGS entrance aperture over a star. Such a scan simultaneously produces one curve for each of the X and Y axes. A good transfer function has a large modulation, which is the left peak to right valley amplitude. An ideal transfer function should have only one positive peak and one negative valley, and so, only one centrally located zero-crossing point. See Bradley et al. (1991), Fig. 6 for an example of a theoretical S curve.

The large spherical aberration of the as-built primary mirror, in the presence of internal FGS misalignments, produces a signature in the transfer functions which mimics coma. Coma causes decreased modulation and multiple peaks and valleys in a transfer function. As discussed in Benedict et al. (1991), the goal of our efforts during 1991 was to find a secondary mirror position (i.e., a secondary mirror tilt and decenter) which would produce excellent S curves in one FGS, good S curves in another, and guiding-capable S curves in the third FGS. At the same time the cameras and spectrographs had their own point spread function requirements. The final *HST* collimation involved some compromise.

We shall first display and discuss the S curves for all three FGS units. These are the product of a year-long collimation campaign. Then, since most astrophysically interesting objects are faint, we will assess the TRANS mode limiting magnitude. Note that all the S curves shown in this paper were taken at the same (final) secondary mirror position.

3.1 Interferometer Response Functions for Bright Stars: The Nine Points of Light Test

Figures 3(a), 3(b), 4(a), 4(b), 5(a), and 5(b) for FGS 1, 2, and 3 show the end result of many months effort by the *HST* Project, the Space Telescope Science Institute, the Astrometry Science Team, and the Instrument Definition

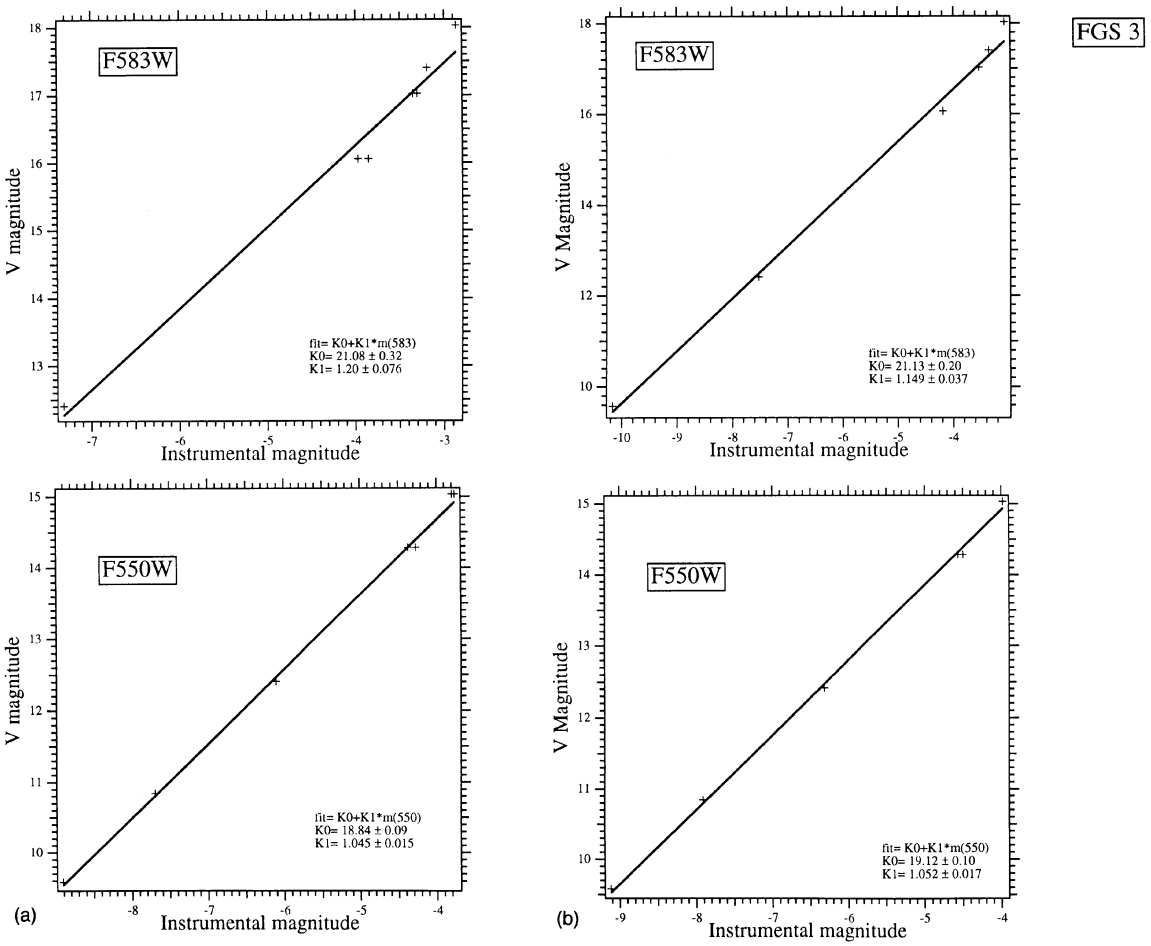

FIG. 2—(a) The Johnson V magnitude vs. the instrumental magnitude for the clear (F583W) and F550W filters for FGS 1. (b) The Johnson V magnitude vs. the instrumental magnitude for the clear (F583W) and F550W filters for FGS 3. In both FGS units, the F550W comparison is better than the unfiltered, an expected result.

Teams. Each S curve in Figs. 3, 4, and 5 was obtained by scanning Upgren-69, while the star was placed at the position within the FGS field of view (hereafter referred to as a "pickle") indicated in Fig. 6. The open and filled spots together constitute a Nine Points of Light test. It is somewhat ironic that these data, taken on day 323 of 1990, demonstrate the best compromise secondary mirror position. It took a year to determine this to our satisfaction.

We present the transfer functions obtained through the F583W, or clear [Figs. 3–5(a)], and the PUPIL [Figs. 3–5(b)] aperture only for the filled spot locations. The PUPIL significantly reduces the aberration effects for each FGS, but also lowers the possible limiting magnitude. Note that FGS 3 (Fig. 5) has the highest-quality S curves in the center of the FGS field of view. This imposes an operational constraint on double-star TRANS mode astrometry. The double and the comparison single star must be observed at the same central location within FGS 3.

Of the three FGS units FGS 2 produces the poorest-quality F583W S curves. The modulation is so low and the S-curve shapes so irregular that all orbital verification tests were modified to exclude FGS 2 from testing. Thus, we report only on FGS 1 and FGS 3 in this paper. A secondary mirror position exists which allows good S curves to be obtained in FGS 2, but the resulting effects on the other *HST* scientific instruments are unacceptable.

Finally, note that the FGS 1 and 2 PUPIL S curves seen in Figs. 3–4(b) are of far better quality than the F583W curves in Figs. 3–4(a). This has produced the operational constraint that all guiding in FGS 1 and 2 is done with PUPIL. And, while the S curves in the center of FGS 3 are of very high quality, this quality is not held over the entire pickle [Fig. 5(a)]. Again, the quality is uniformly higher for the PUPIL results shown in Fig. 5(b). Since guide stars can be found in all locations within a pickle, the evidence collected by comparing Figs. 3–5(a) with Figs. 3–5(b) has forced *HST* to use brighter guide stars than the original $V=14.5$ limit in all FGS units.

As we see, no FGS produces an ideal S curve. Nonetheless, TRANS mode scientific results can be obtained. Franz et al. (1991) present a successful TRANS mode observation of a relatively bright binary star, ADS 11300. For this pair, the primary has $V=8.8$. Obtaining the S curves using the central region of FGS 3 and the PUPIL

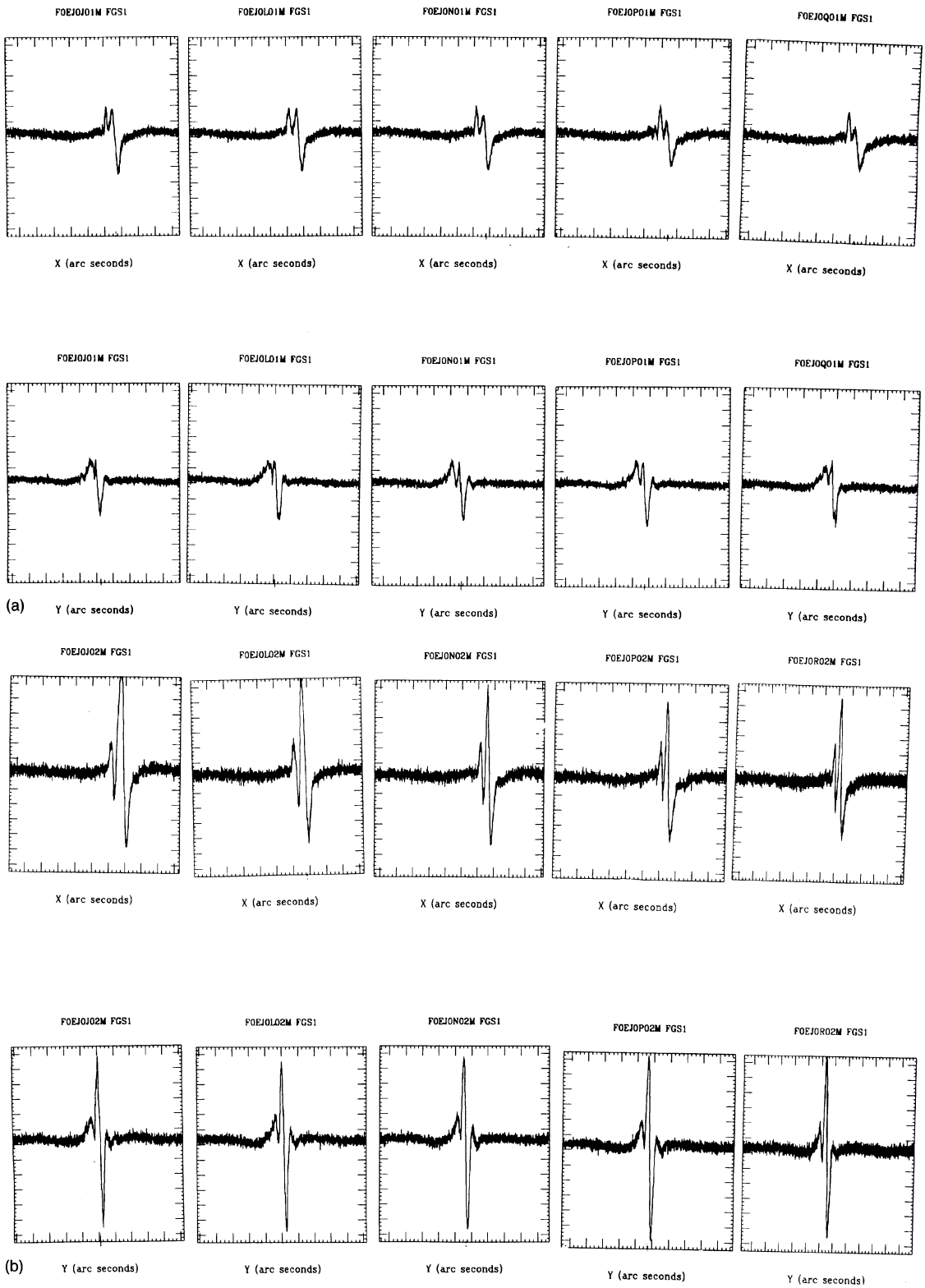

FIG. 3—(a) F583W (clear filter) interferometer response functions within FGS 1, X axis at the top, Y axis at the bottom. Each S curve is an average of five separate scans. These are partial results from a Nine Points of Light test, displaying the S curves within each pickle at the locations mapped in Fig. 6. The S curves are displayed in clockwise sequence (with the pickle concave downward). For each S curve in Figs. 3–5 Upgren-69 was the target star and the *HST* secondary mirror was in the final collimation position. The x and y scales are the same within each graph, $\Delta x = 1.8$ arcsec and $-0.8 < y < 0.8$. The transfer scans have the same, far from ideal, shape over the entire pickle. (b) PUPIL interferometer response function for FGS 1. The use of an aperture stop has greatly reduced the effects of spherical aberration, increasing the modulation of the pattern and reducing the modulation of the secondary peaks.

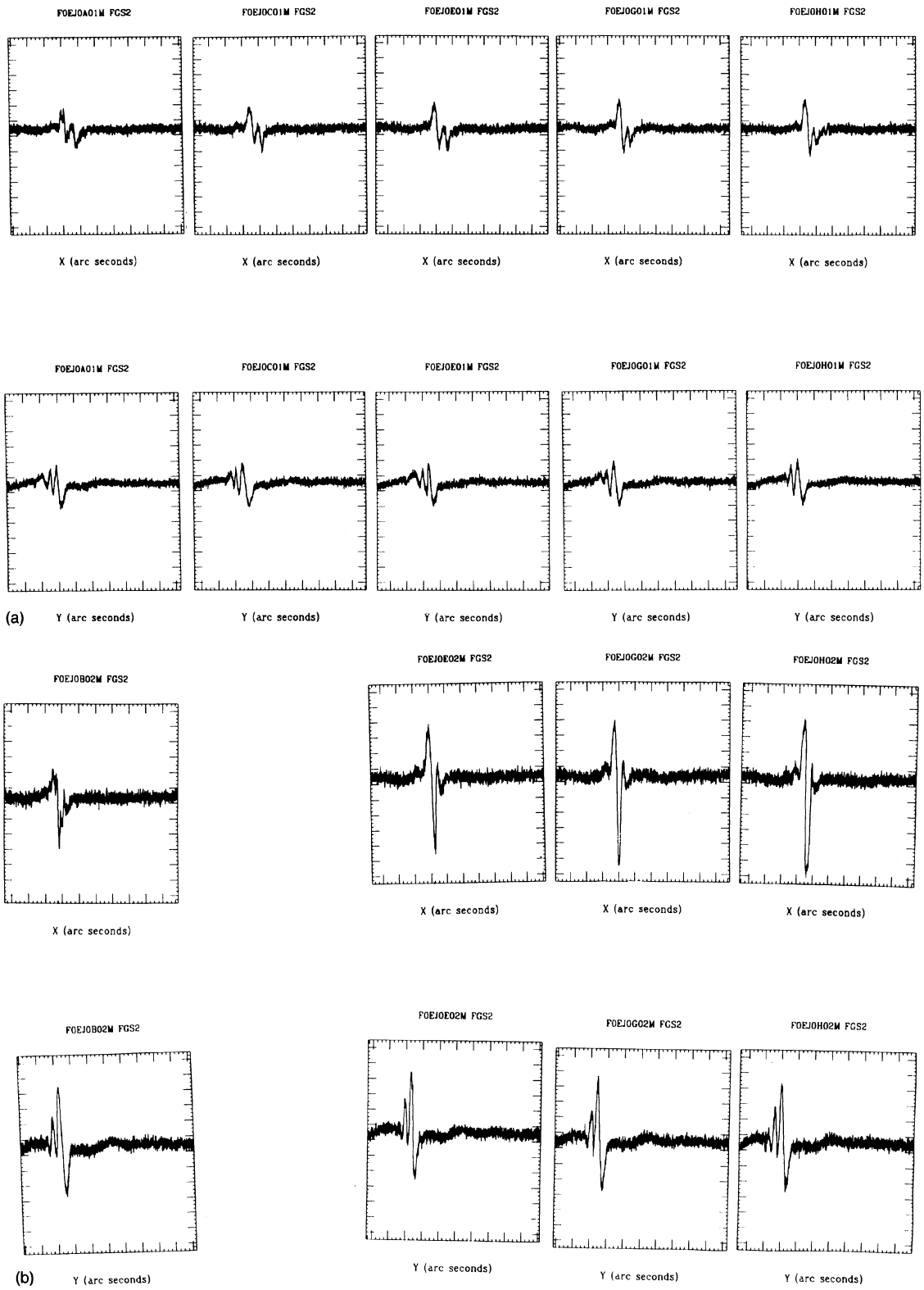

FIG. 4—(a) F583W (clear filter) interferometer response function for FGS 2. These are uniformly the poorest *S* curves. (b) PUPIL interferometer response function for FGS 2. The introduction of the aperture stop has improved the *S*-curve characteristics. Most are somewhat better than the FGS 1 F583W results. Gaps in our coverage were due to guide-star loss of lock produced by *HST* jitter.

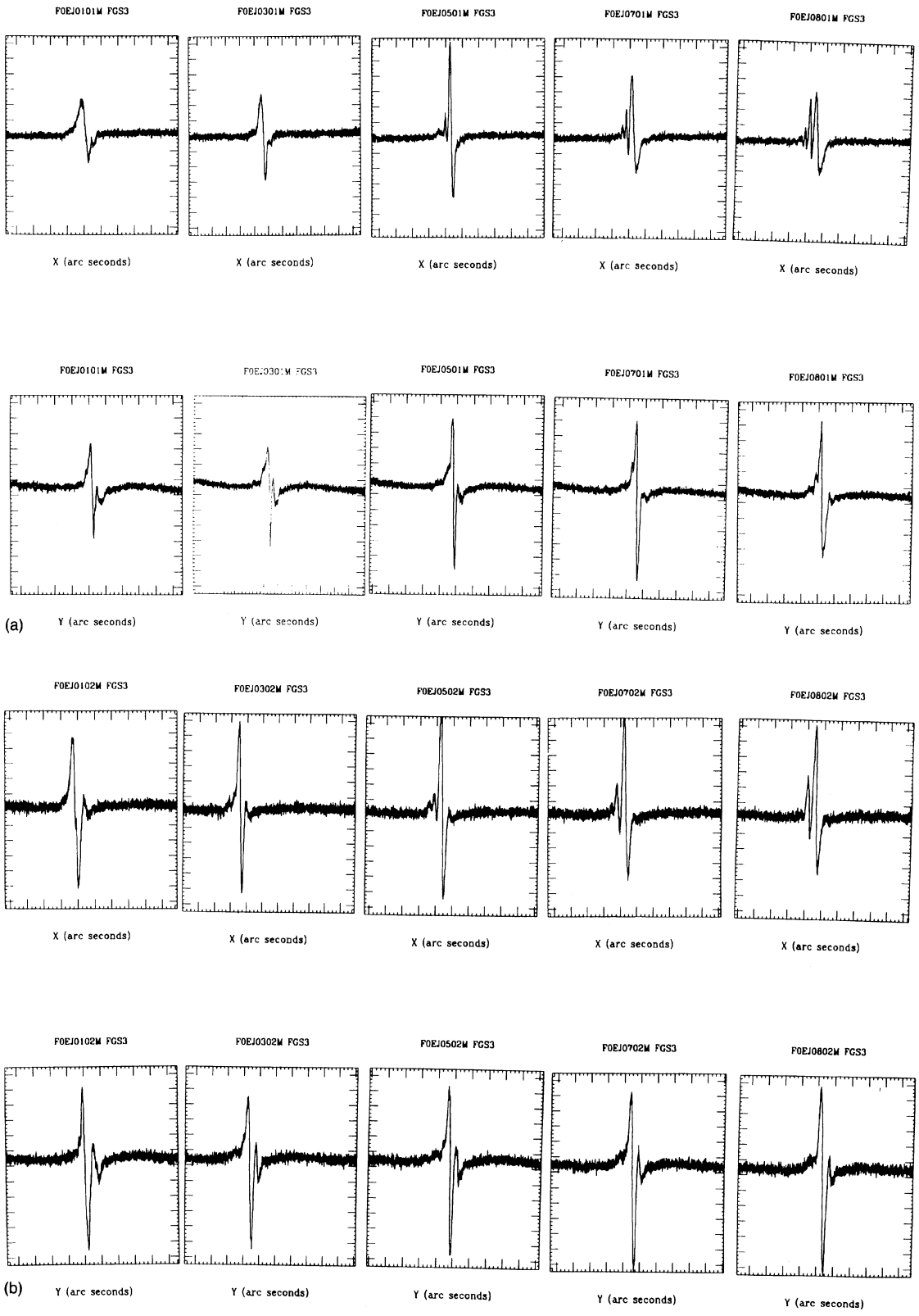

FIG. 5—(a) F583W (clear filter) interferometer response function for FGS 3. The central position provides the highest-quality response function of any FGS. Note the variation in *S*-curve shape and quality across the pickle. (b) PUPIL interferometer response function for FGS 3. We find good-quality *S* curves for the entire pickle, but still see variations as a function of position within FGS 3.

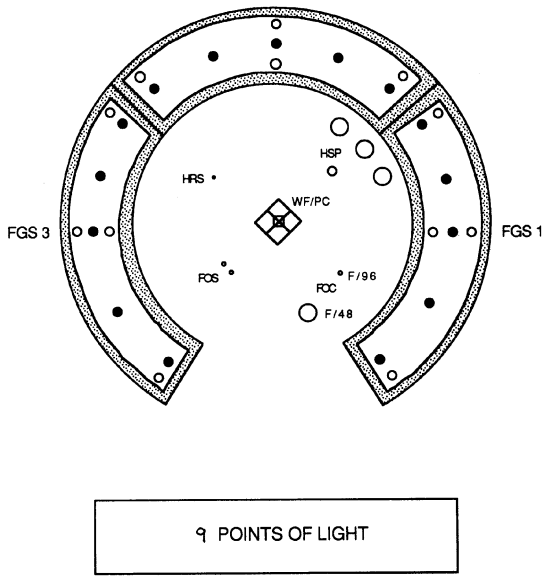

FIG. 6—The *HST* focal plane. The locations of the *S* curves presented in Figs. 3–5 are indicated by filled spots within each pickle. Data for Figs. 3–5 were obtained at all spot locations in a Nine Points of Light test. We show results only for five locations.

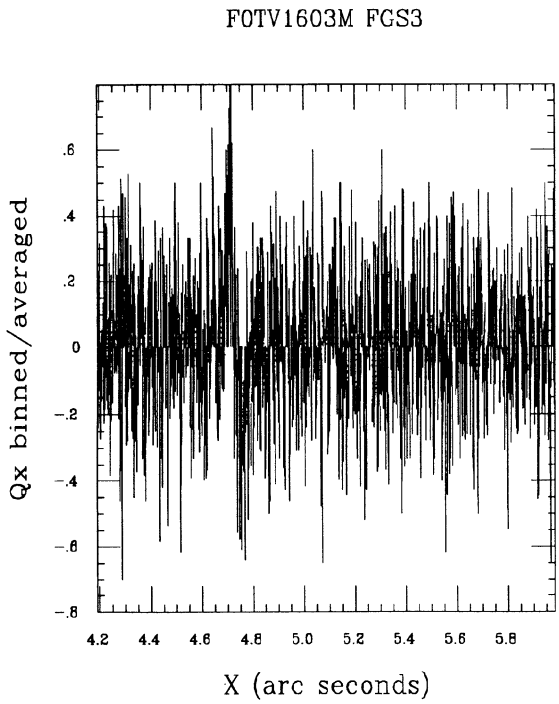

FIG. 7—The *X* component of a single transfer scan across Sandage-I95, $V=16.06$ obtained in the center of FGS 3. The interferometer response is just visible at $X=4.7$ arcsec.

aperture we resolved a binary with $\Delta m=0.41\pm0.07$ mag and $\Delta r=0.066\pm0.003$ arcsec. These observations were acquired with a somewhat different secondary mirror position than the position which resulted in the Figs. 3–5 *S* curves. This presents no problems, because the comparison single star was also observed at that same secondary mirror position.

Since the modulation and even the detectability of the transfer function decrease as the noise increases (i.e., we observe fainter stars), one of our major concerns was the *S*-curve quality for faint stars. We now address this issue.

3.2 Faint Star in FGS 3

To determine the limiting magnitude for TRANS mode astrometry, we planned to observe each of stars 6, 7, and 10 (Table 1) using first F583W then the PUPIL aperture. Each complete TRANS mode observation consisted of 15 scans across the star. Of the six attempted TRANS mode observations, only one, an F583W observation of Sandage-I95 ($V=16.06$) resulted in *S* curves for both axes. For the PUPIL observation of Sandage-I95, one of the user-selectable *K* factors, acting as a count detection limit for star presence, was set too high. So the coarse track did not properly center the target star. Thus, these PUPIL TRANS scans were done at the wrong location. Nonetheless, we did see the star along the *Y* axis. Of the remaining TRANS observations, one was corrupted by a terminator crossing. For the remaining three observations our detection-limit *K* factors were incorrect, and the stars were not acquired.

The software which produces the command load sent up to *HST* inserted incorrect detection-limit *K* factors for every observation in every FGS reported on in this paper, TRANS and POS mode. These values, based on prelaunch ground testing, were uniformly too high. The command load is called a Science Mission Schedule (SMS). The Astrometry Team was able to edit these SMSs (in some cases mere hours before they were sent up to *HST*) and insert correct values for most of the detection limit *K* factors. However, our editing algorithm missed the TRANS mode observations and several bright stars POS-mode observations. Hence, we failed the TRANS mode detection limit for all but the brightest magnitude limit star, Sandage-I95. Nonetheless, we consider the *K*-factor correction campaign a great success. Without this effort, we would have no successful observations (POS or TRANS mode) for any stars fainter than $V=13$.

In spite of all these problems we can estimate a limiting magnitude, using the successful F583W and partially successful PUPIL TRANS observations of Sandage-I95. Figure 7 presents the *X* component for 1 scan out of 15 for the F583W observation. The *S* curve is barely visible through the noise. Figure 8(a) displays an easily recognizable *X*-component *S* curve. Figure 8(b) displays the corresponding *Y S* curve. These *S* curves were produced by averaging the 15 scans making up the complete TRANS observation. We then boxcar binned each average *S* curve with a window 4 pixels wide. This mimics a single scan done with a Fine Error Signal averaging of 1.6 s per data point and corresponds to the required walkdown averaging for a star of this brightness (Bradley et al. 1991). No effort was made to register (de-jitter) the individual scans before the

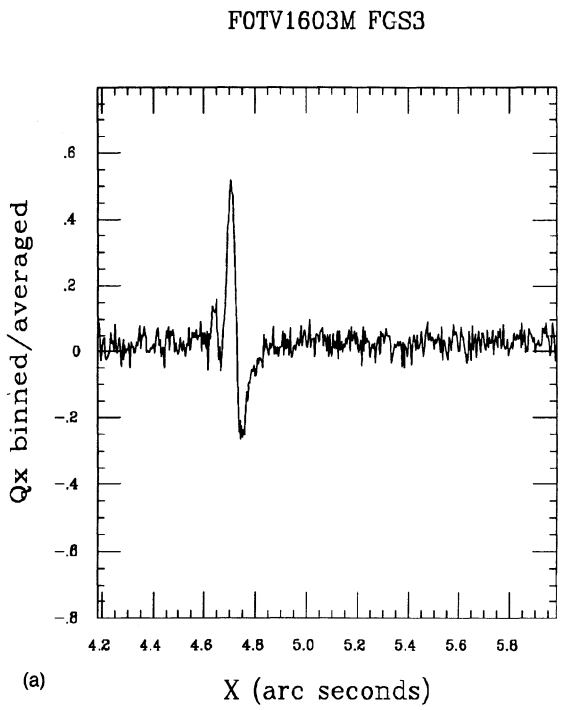

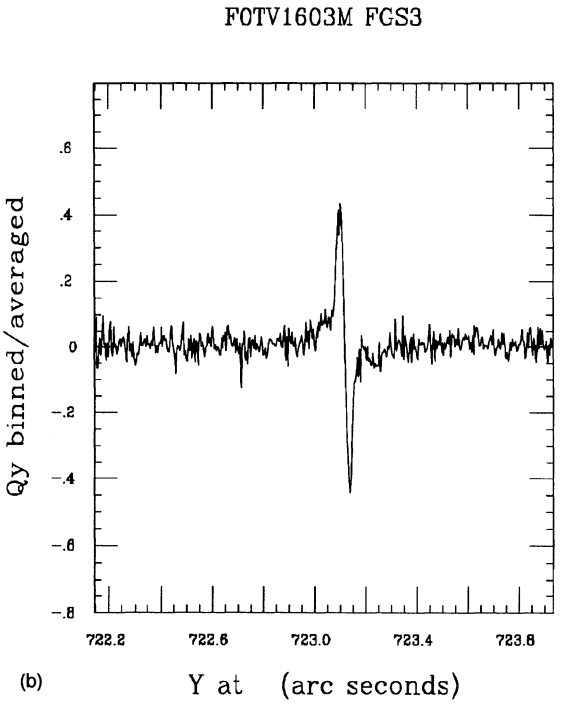

FIG. 8—The processed (a) X-component and (b) Y-component F583W S curves for Sandage-I95, $V=16.06$ obtained in the center of FGS 3. These result from an average of all 15 scans acquired during the observation. The final S curves have been boxcar smoothed with a 4-pixel-wide kernel. This treatment produces S curves equivalent to those acquired with FES averaging of 1.6 s. Comparing with the FGS 3 F583W bright-star S curve in Fig. 5(a), we find the modulation somewhat decreased (due to smoothing and uncompensated jitter), but the shapes are preserved. We conclude that binary-star astrometry like that in Franz et al. 1991 would be possible in FGS 3.

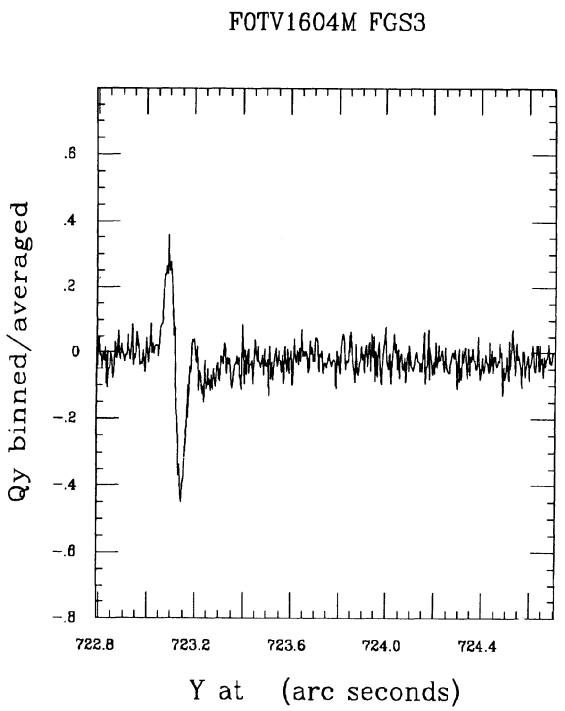

FIG. 9—A Y-component PUPIL S curve for Sandage-I95, $V=16.06$ obtained in the center of FGS 3, processed in the same way as the results presented in Fig. 8. Comparing with the FGS 3 PUPIL bright-star S curve in Fig. 5(b), we again find decreased modulation, but a similar shape.

averaging process. We simply stacked the 15 scans. Comparing the faint-star S curve (Fig. 8) with the corresponding bright-star S curve [Fig. 5(a), central S curve], we note the similarity and conclude that TRANS mode astrometry can be done on $V=16$ stars. The modulation is somewhat less for the faint star. This we attribute to the averaging and smoothing. Figure 9, the Y component of a PUPIL observation of the same star processed in a similar fashion, argues that we might successfully observe $V=16.8$ stars in the central region of FGS 3. In this case we compare Fig. 9 with the central PUPIL observation in Fig. 5(b) and point out that the PUPIL and F583W S curves are very similar at this location.

3.3 Faint Star in FGS 1

To determine the TRANS mode-limiting magnitude in FGS 1, the same stars used for FGS 3 above were observed with much the same results. Between jitter-induced loss of lock and erroneous K factors we secured only one successful observation out of six attempted. We obtained a complete data set for Sandage-I95 ($V=16.06$) with the PUPIL aperture.

Figures 10(a) and 10(b) presents the final FGS 1 X and Y S curves produced in exactly the same manner as for FGS 3. Comparing these results with the corresponding central bright-star PUPIL S curve in Fig. 3(b), we note some degradation due to jitter, especially in the minimum to the right of the central zero crossing. Figure 10(b)

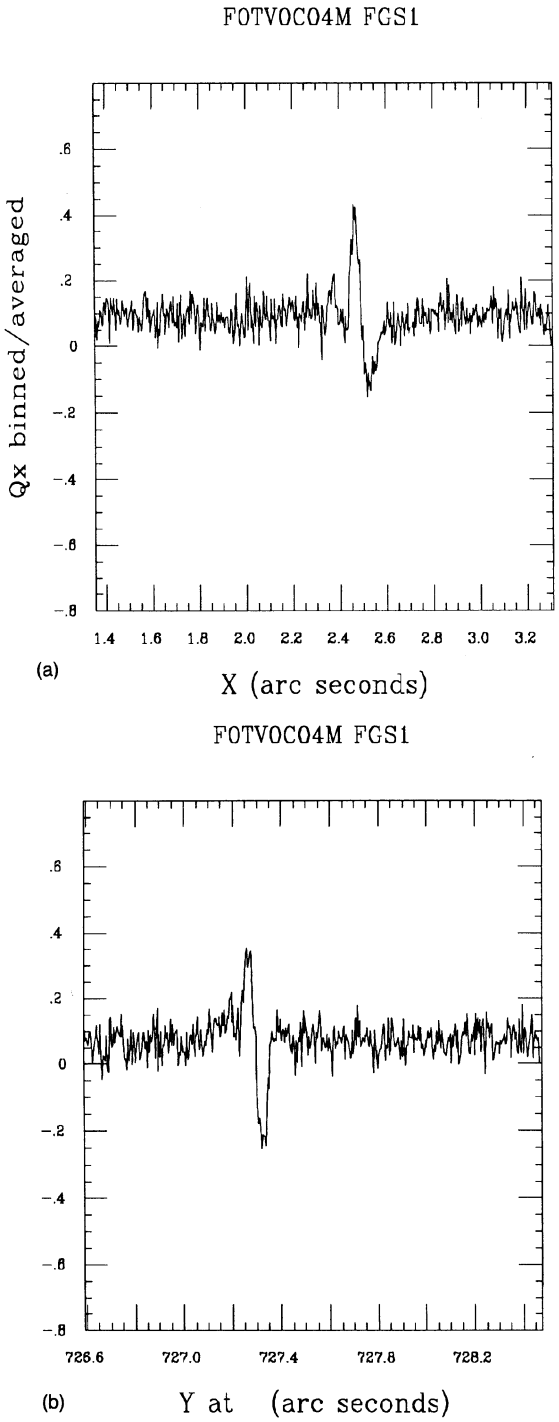

FIG. 10—The processed (a) *X*-component and (b) *Y*-component PUPIL *S* curves for Sandage-I95, $V=16.06$ obtained in the center of FGS 1.

shows lower overall modulation due to jitter, averaging, and smoothing. We conclude that FGS 1 could provide successful TRANS mode observations for stars of $V<16.1$.

4. POS MODE

POS-mode observations consist of a series of star-selector encoder readings taken while the on-board FGS electronics strives to detect and follow the central zero-crossing point (or null) of the *S* curve in, e.g., Fig. 8(a). Tables 4 and 5 list the stars successfully observed during the POS-mode Astrometry Orbital Verification test for FGS 3 and 1, respectively. A successful astrometry observation requires active fine-lock guidance from both guide stars. Many of the failed observations (not listed in Tables 4 and 5) were due to loss of fine lock. The tables include the target ID from Table 1, the *V* magnitude, the measured position and associated standard deviation, the time of observation, the Fine Error Signal averaging period in seconds, and the commanded and the actual exposure time in seconds. The *X* and *Y* positions are derived from the star-selector encoder readings during normal astrometry post-observation pipeline processing. These are the star-selector encoder readings (θ_a and θ_b illustrated in Fig. 3, Bradley et al. 1991) transformed to a Cartesian coordinate system with *X* origin at the center of each pickle. On the sky in each pickle positive *Y* is outward from an origin at the center of the *HST* field of view. Positive *X* points in the counterclockwise direction within each pickle. These axes are aligned along the spacecraft *V*1, *V*2, and *V*3 axes as shown in Bradley et al. (Fig. 2). In particular FGS 3 *Y* is aligned with spacecraft *V*2.

Note that in each case the actual exposure time was longer than the commanded exposure time. The commanding system requires that sufficient time be allocated for a worst-case acquisition. These observations are commanded in absolute time with a certain amount of safety time overhead which is dependent on star magnitude, fine error signal averaging period, and walkdown length. Usually the target is acquired early, resulting in increased time on target.

The POS-mode observations in Tables 4 and 5 are grouped by orbit. Within each orbit, a single pair of guide stars was used. Each observation was planned to occur at the center of the FGS unit being tested. The position differences from orbit to orbit are immaterial. Drifts of 1 arcsec are to be expected between Guide Star acquisitions. Position differences within each orbit are an indication of the POS-mode measurement accuracy and are generally the same size as σ_x and σ_y, but not always. We attribute these small differences to the fact that the positions in Tables 4 and 5 have not been corrected for differential velocity aberrations caused by *HST* orbital motion, nor for possible relative positional shifts introduced by the use of different filters.

4.1 FGS 3

Table 4 presents a list of all the successful FGS 3 POS-mode observations acquired during the Astrometry Verification test. These were made starting on day 359 of 1991. Out of 37 attempts at fine lock POS-mode observations, 4 were affected by jitter-induced loss of guide-star fine lock. Six target observations were degraded by jitter occurring at terminator crossing. Seven observations failed because the count rate was too low (faint star, faint star observed with PUPIL, or star observed with F5ND). We note that the

TABLE 4
FGS 3 POS Mode Results

	ID	V	Filter	X (arcsec)	Y (arcsec)	sX (arcsec)	sY (arcsec)	OBS T	FES T (sec)	EXP (sec)	actual EXP (sec)
1	Upgren-111	12.41	F583W	5.4325	726.2195	0.0019	0.0026	10:26:52	0.025	60	100.35
2	Upgren-111	12.41	F605W	5.4379	726.2313	0.0028	0.0020	10:38:53	0.1	60	81.45
3	Upgren-111	12.41	F550W	5.4336	726.2307	0.0019	0.0023	10:41:09	0.1	60	80.85
4	Upgren-111	12.41	PUPIL	5.4342	726.2235	0.0017	0.0024	10:43:19	0.05	60	77.40
5	Upgren-112	10.84	F550W	5.8083	726.8494	0.0019	0.0031	12:03:38	0.05	60	101.55
6	Upgren-111	12.41	F550W	5.3859	726.2795	0.0019	0.0030	13:27:00	0.05	60	107.10
7	Upgren-111	12.41	F550W	5.3864	726.2787	0.0019	0.0029	13:30:06	0.2	60	83.85
8	Upgren-108	15.03	F550W	5.4020	726.1275	0.0040	0.0047	14:01:28	0.2	60	110.55
9	Upgren-112	10.84	PUPIL	4.1320	726.8283	0.0022	0.0031	15:16:31	0.025	60	101.40
10	Upgren-111	12.41	PUPIL	4.6038	727.0945	0.0018	0.0028	16:40:00	0.05	60	105.60
11	Upgren-111	12.41	PUPIL	4.6053	727.0947	0.0021	0.0020	16:43:09	0.2	60	80.40
12	Upgren-108	15.03	PUPIL	4.6551	726.9406	0.0029	0.0038	18:17:14	0.2	60	108.30
13	Upgren-108	15.03	F550W	4.6585	726.9499	0.0028	0.0017	18:25:09	1.6	60	131.55
14	Upgren-108	15.03	PUPIL	4.6556	726.9408	0.0023	0.0016	18:31:13	1.6	60	117.75
15	Sandage-I118	17.02	F583W	4.0824	727.9982	0.0032	0.0058	20:05:01	3.2	120	258.45
16	Sandage-I95	16.06	F583W	4.7259	723.0957	0.0024	0.0032	5:38:16	1.6	90	168.00
17	Sandage-I95	16.06	PUPIL	4.7317	723.0965	0.0023	0.0028	5:51:37	3.2	120	191.40
18	Sandage-I118	17.02	F583W	4.5308	727.2045	0.0033	0.0025	9:11:38	3.2	120	189.45
19	Sandage-I95	16.06	F583W	4.0315	723.6614	0.0032	0.0043	10:42:13	1.6	120	200.85
20	Sandage-I95	16.06	PUPIL	4.0339	723.7639	0.0057	0.0029	10:55:49	3.2	120	193.80

guide stars used for these observations were fainter than the nominal limit. One guide star had $V=13.7$.

All of the POS-mode data discussed in this section were acquired in the middle of each pickle. Inspection of Figs. 3(a) and 5(a) shows that while the non-PUPIL interferometer response function for FGS 1 has the same shape throughout the pickle, this is not the case for FGS 3. Hence, the F583W limiting magnitude and positional accuracies presented below for FGS 3 should be considered the best possible.

Figure 11 presents a plot of the X versus Y positions for an F550W POS-mode observation of Upgren-111, $V=12.41$, consisting of 3205 individual readings. We call this representation a jitter ball. For this successful observation most of the jitter is specific to the astrometry FGS. The honeycomb structure shows that we resolve the least significant bit in the star-selector encoders.

4.1.1 FGS 3 Limiting Magnitude

Table 1 lists our limiting magnitude check stars (those from Sandage 1962) which ranged $16.06 \leqslant V \leqslant 18.03$. Each faint star was observed on two different orbits to confirm acquisition. If we define successful astrometry as having internal errors of position of <0.003 arcsec (standard deviation), from Table 4 we see our F583W limiting magnitude in FGS 3 is $V=17$. We astrometrically detect Sandage-I118. Figure 12 shows the jitter balls for the two independent observations of Sandage-I118, $V=17.02$. The top jitter ball contains information from the 10,387 individual measures which define this observation. However, since we commanded a Fine Error Signal averaging period of 3.2 s, only 86 unique readings are returned for ground processing. The bottom observation consisted of 7627 measures, collapsed to 60 unique readings.

TABLE 5
FGS 1 POS Mode Results

	ID	V	Filter	X (arcsec)	Y (arcsec)	sX (arcsec)	sY (arcsec)	OBS T	FES (sec)	EXP (sec)	actual EXP (sec)
1	Upgren-112	10.84	PUPIL	1.4930	724.8696	0.0025	0.0045	13:28:22	0.025	60	100.35
2	Upgren-112	10.84	PUPIL	1.4910	724.8701	0.0049	0.0016	13:30:49	0.05	60	73.5
3	Upgren-108	15.03	PUPIL	0.9230	724.9786	0.0037	0.0057	16:17:11	0.2	60	109.5
4	Upgren-108	15.03	F550W	0.9160	724.9769	0.0039	0.0038	16:25:00	1.6	60	128.85
5	Upgren-108	15.03	PUPIL	0.9190	724.9868	0.0022	0.0020	16:30:53	1.6	60	122.4
6	Sandage-I95	16.06	F583W	2.3570	727.1578	0.0077	0.0069	6:48:02	1.6	120	173.55
7	Sandage-I95	16.06	PUPIL	2.3820	727.1711	0.0034	0.0030	7:02:31	3.2	120	193.05

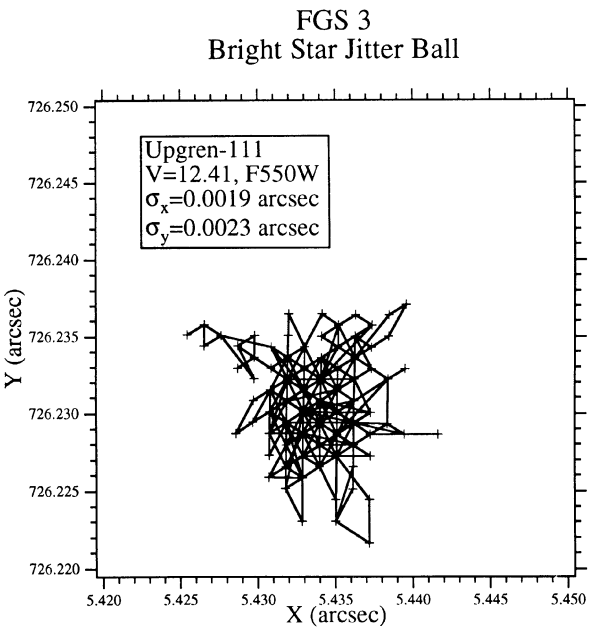

FIG. 11—X versus Y (jitter ball) for a FGS 3 POS mode observation made through an F550W filter (line 3, Table 4). Star has $V=12.41$. The standard deviations are as indicated. Guiding was done in fine-lock mode with the PUPIL aperture.

The jitter-ball display draws one's attention to the maximum excursions taking place during an observation. Particularly for the top jitter ball in Fig. 12, the FGS remained at the extremes for very little time. Note that $\sigma_y > \sigma_x$. Figure 13 demonstrates why $\sigma_y > \sigma_x$ and demonstrates the reason for the extreme excursions. We plot the line of sight jitter along the X and Y axes for FGS 1, one of the guiding FGS. Spacecraft jitter is obviously greater along the FGS 3 Y axis. This axis is co-linear with the spacecraft $V2$ axis (Bradley et al. 1991, Fig. 2).

We stress, again, that this derived limiting magnitude is only valid for the center of the pickle. Given the S-curve variations within FGS 3 [Fig. 5(a)], we are not likely to reach $V=17$ near the ends of the pickle.

4.1.2 FGS 3 Position Measurement Precision

We plot all the formal position errors in Table 4 against V in Fig. 14. In this plot we distinguish between PUPIL and F583W (clear aperture) observations. Note that in most cases the Y error is larger than the X. This reflects the effects of *HST* spacecraft jitter, which is primarily along the Y axis of FGS 3. For all measurements we obtain average standard deviations $\langle\sigma_x\rangle=0.0026$ and $\langle\sigma_y\rangle = 0.0029$ arcsec. It is apparent that, particularly for the fainter stars, the measurement errors are less for PUPIL observations than for any full-aperture observations of the same star.

4.1.3 FGS 3 FES Averaging

It is possible to perform on-board averaging of the fine-error signal. Instead of receiving a position each 0.025 s, it is possible to average 2^n samples, where $0 < n < 7$. Thus, the averaging period can be as long as 3.2 s. This could provide higher-quality data, especially for fainter stars. The penalty for use is a longer walkdown time (Bradley et al. 1991, Sec. 3.4). Comparing lines 12 and 14 and lines 8 and 13 in Table 4, we see that FES averaging does generally have the expected effect. The standard deviations drop.

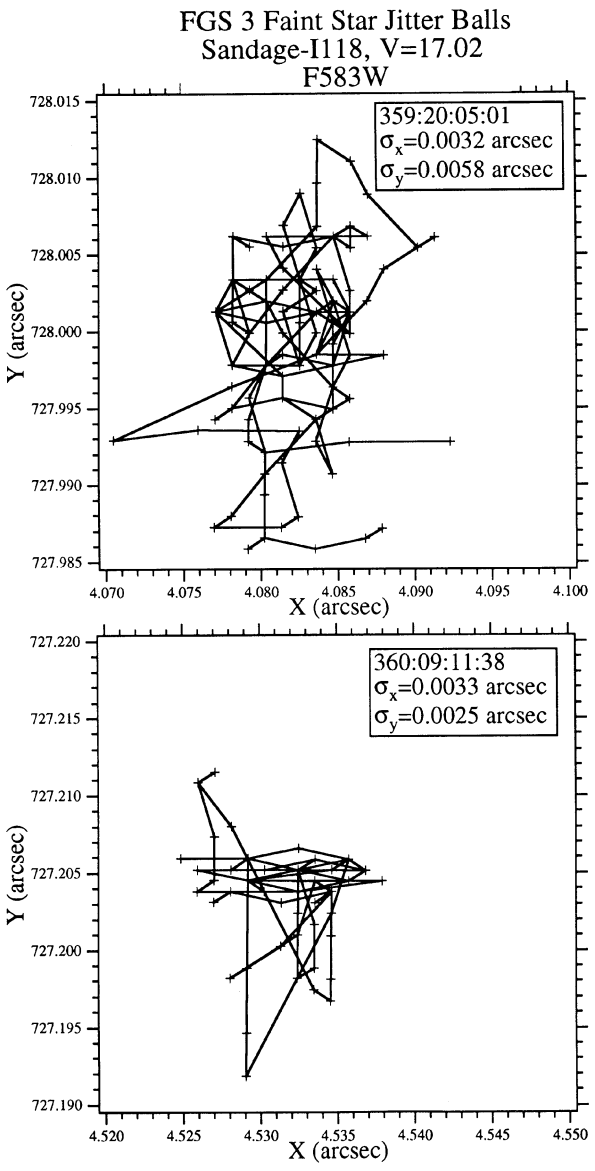

FIG. 12—We compare two FGS 3 F583W observation jitter balls for a faint star, $V=17.02$. The distributions within the jitter balls and the formal standard deviations argue that we have obtained valid astrometric measurements for this star on two occasions separated by 12 h. The time stamps in the legends are day number within 1991 and UT. Guiding was done in fine-lock mode with the PUPIL aperture.

4.2 FGS 1

Table 5 presents a list of all the successful POS-mode observations acquired by FGS 1 during the Astrometry Verification test, again, grouped by orbit. The observations

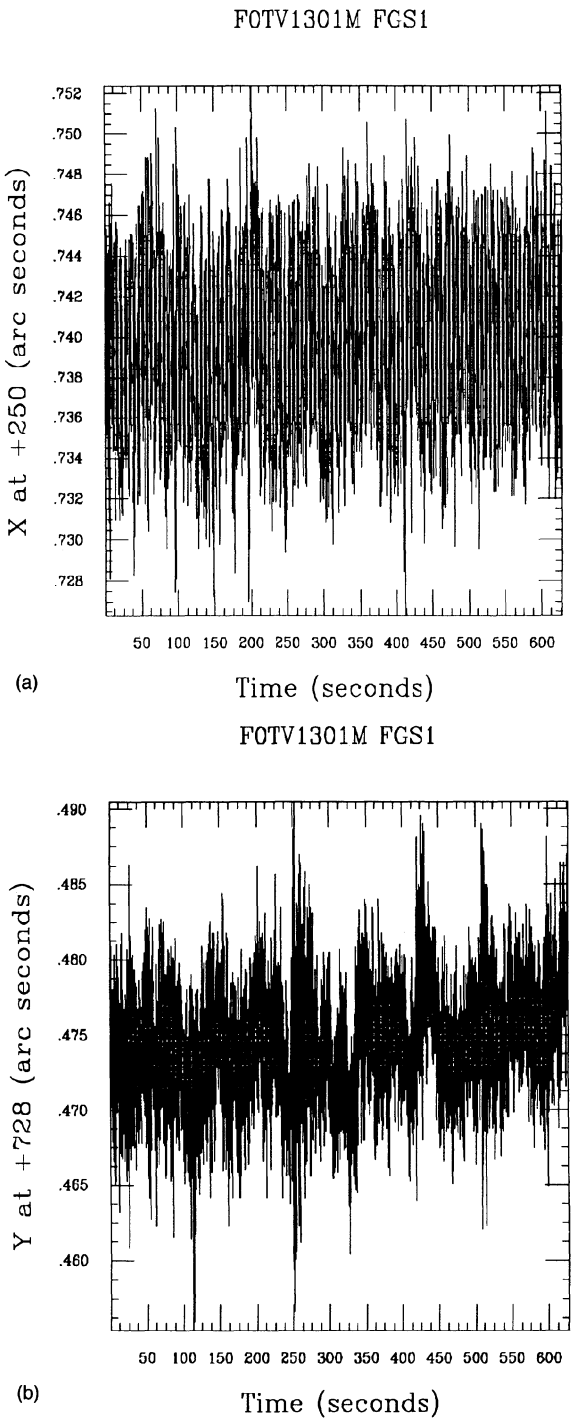

FIG. 13—(a) X and (b) Y line-of-sight jitter as reported by the guiding FGS 1 prior to and during the top observation (duration 258 s) shown in Fig. 12. The FGS 3 observations start at about time=367 s and ends at the right of the plot, time=625 s. Guiding was done in fine-lock mode with the PUPIL aperture. Note that the y-axis scales differ and that the Y-axis jitter is obviously larger than the X axis. This guide star had $V \approx 13$.

were made starting on day 354 of 1991. Out of 37 attempts at fine lock, 17 were ruined by jitter-induced loss of guide-star fine lock. Five observations were degraded by jitter. Four attempts failed because the count rate was too low

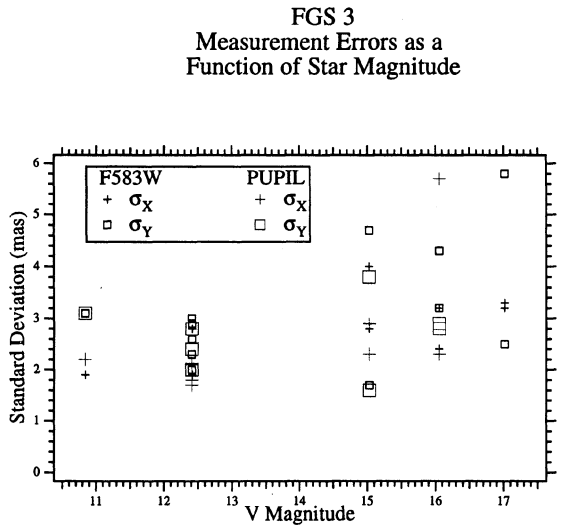

FIG. 14—Standard deviations in milliarcsec (mas) for all FGS 3 POS mode PUPIL and F583W measurements (listed in Table 4) are plotted against target star V magnitude. PUPIL observations seem to have marginally smaller errors.

(faint star, faint star observed with PUPIL, or star observed with F5ND). Four observations had improperly set star detection limits.

4.2.1 FGS 1 Limiting Magnitude

We, again, define successful astrometry as having internal errors of position of <0.003 arcsec (standard deviation). In Table 5 we list the successful acquisition and measurement of a $V=16.06$ star (Sandage-I95) through the F583W (clear) and PUPIL. While the fainter stars were detected in the PMT counts [F583W, Fig. 2(b)], either the standard deviations were in the 0.10-arcsec range, or there was no fine lock achieved. From Fig. 3, we know that in FGS 1 the PUPIL S curve is of far higher quality than the F583W. Any astrometry done in FGS 1 would likely use the PUPIL aperture. This choice is supported by comparing the standard deviations for the two Sandage-I95 observations in Table 5. Hence, we tentatively choose a limiting magnitude of $V=16.1$. This is likely to be the limiting magnitude throughout the entire FGS 1 FOV, since the PUPIL interferometer response function is the same everywhere in this pickle, as shown in Fig. 3(b).

4.2.2 FGS 1 Position Measurement Precision

For all measurements in Table 5, we find these average standard deviations: $\langle \sigma_x \rangle = 0.0040$ and $\langle \sigma_y \rangle = 0.0039$ arcsec. That the average accuracy is worse for FGS 1 we attribute to the lower-quality S curves, obvious in Fig. 3(a). Again, from Table 5 it is apparent that in most cases the measurement errors are less for PUPIL observations than for any full-aperture observations of the same star. The higher-quality S curves resulting from the use of the PUPIL aperture [Fig. 3(b)] are expected to give better results.

4.2.3 FGS 1 FES Averaging

Comparing lines 3 and 5 in Table 5, we see that FES averaging again has the expected effect. The errors drop.

One final point: comparing the FGS 1 and FGS 3 POS-mode results with the bright-star TRANS mode results can convince one that good *S* curves imply good POS-mode performance. Conversely, poor *S* curves degrade POS-mode performance.

5. FINE ERROR SIGNAL GAIN

Operation of the FGSs for astrometry requires several parameters to be set in the FGS electronics. These parameters are uplinked and will vary from default values used for "regular" guiding, and may vary for special guiding problems, as well as for astrometric use. We had hoped to vary the uplink parameter K1, which is the gain used to calculate the Fine Error Signal from the linear portion of the *S* curve. There is a separate gain for each axis (Bradley et al. 1991, Sec. 2.3.2). The optimum values for these gains will depend on the height of the *S* curve, which, in turn, depends on the optical characteristics of each axis of each FGS. As we have seen (Figs. 3–5), *S*-curve height depends on the FGS unit, the aperture, and, in the case of FGS 3, varies within the pickle.

Additionally, these gains might depend on the specific object being observed. An extended object will reduce the amplitude of the *S* curve, as will the presence of another star in the 5-arcsec-square aperture along with the target, as will stray light or background nebulosity. Therefore, the effects of changing the gain must be determined for each FGS axis. In some cases, using an incorrect K1 value may reduce efficiency. In others, it may make the difference between obtaining and not obtaining an observation.

Unfortunately, this section of the astrometry verification test was completely wiped out by the inability of *HST* to provide a stable observing platform. We hope to modify some future Science Verification test to include K1 fine-tuning.

6. SHORT-TERM THERMAL STABILITY

To test for effects caused by thermal variations, we observed a set of stars in round-robin fashion over seven orbits, holding the *HST* orientation and pointing as constant as the Pointing Control System would allow. The target field is shown in Fig. 15, along with the guide stars used for the entire set of observations. Temperature changes within FGS 2 are particularly important. Given its location within *HST*, the FGS 2 housing receives the most sunlight. This heating and the poor-quality *S* curves are a serious potential threat to fine-lock guiding.

The thermal changes explored below are quite typical of normal *HST* operations. The monitored temperatures included the *HST* aft shroud, the FGS forward radiator, and the FGS star-selector motor encoder temperatures. The aft shroud is the skin of *HST* covering the section containing the FGS units.

The forward radiator temperature sensor is located near the pick-off mirror in the lower left-hand corner of Fig. 2 in

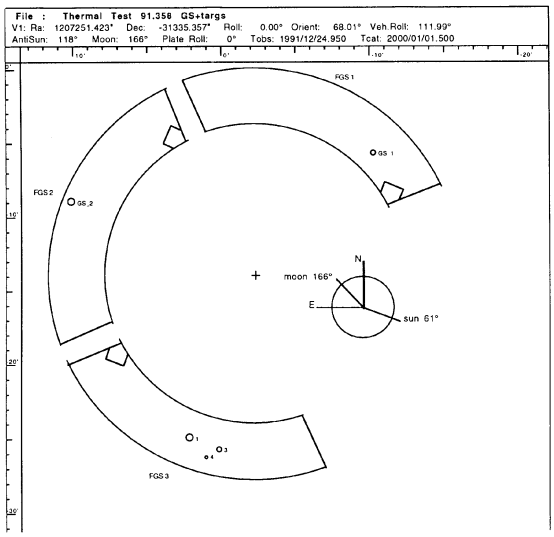

FIG. 15—*HST* orientation, guide stars, and target stars for the short-term thermal stability test are displayed using Pickles (McCartney et al. 1990). The targets are in FGS 3.

Bradley et al. (1991). The pick-off mirror is at the *HST* focal plane. This temperature provides an indication of the average internal FGS thermal environment. Measurement of the radiator temperature indicates the amount of thermal energy being dumped to the external environment. When the temperature sensor yields readings within established limits, most of the FGS internal electro-optical train can be considered to be in thermal equilibrium. When this sensor violates the upper limit, either internal problems have arisen due to heaters, or more than a nominal amount of thermal energy from sunlight on the aft shroud is being dumped through the radiator.

The third sensor monitors a housing within each FGS unit containing the star selectors and the corrector group. We saw no variations in star-selector motor encoder temperatures for any FGS. They remained constant at 20.9 ±0.2 C. The aft shroud temperature varied as shown in Fig. 16(a). Forward radiator temperature variations did occur, as shown in Fig. 16(b).

Positions and magnitudes for the observed stars (from the GSSS, Lasker et al. 1990) are shown in Table 3. A complete list of the successful observations with associated errors (standard deviations) can be found in Table 6. Note that in most cases, the *Y* standard deviation is larger than the *X*, likely attributable to jitter. The observations were obtained in FGS 3 using the PUPIL aperture and all guided in fine lock by FGS 1 and 2.

Of 13 sets of three observations (39 individual observations) spaced over 10 h, three sets were ruined by spacecraft jitter, induced by solar array flexure at terminator crossings. Most of these data were secured during orbit day. Spacecraft jitter, excited by terminator crossings, can affect observations throughout an orbit. For example, we experienced only one terminator crossing during an observation set. Yet, three sets were rendered unusable by jitter.

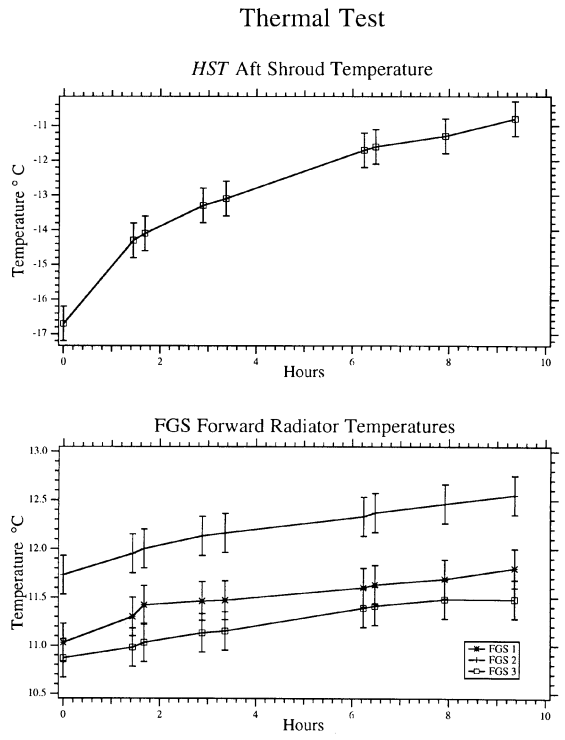

FIG. 16—Temperatures monitored during the thermal test included (top) the *HST* aft shroud and (bottom) the FGS forward radiator.

Our final test material consists of ten sets of POS-mode observations for three stars covering a time span of 9.9 h. All these positional data were corrected for spacecraft-velocity aberration, using the predicted orbit.

TABLE 6
Thermal Test Log of Observations

set ID	star ID	V	elapsed time (hours)	X (arcsec)	Y (arcsec)	sX (arcsec)	sY (arcsec)	T exp (sec)
1	1	10.65	0.00	6.3551	725.1521	0.0022	0.0026	194.25
	3	11.16	0.14	139.2054	726.6413	0.0024	0.0030	168.30
	4	14.01	0.22	101.4969	772.0000	0.0047	0.0068	173.55
2	1	10.65	1.35	6.3573	725.1545	0.0026	0.0042	195.60
	3	11.16	1.50	139.2079	726.6416	0.0025	0.0028	168.15
	4	14.01	1.57	101.4981	772.0017	0.0021	0.0024	173.70
3	1	10.65	1.64	6.3548	725.1499	0.0021	0.0032	168.30
	3	11.16	1.77	139.2048	726.6393	0.0024	0.0029	168.30
	4	14.01	1.85	101.4949	771.9980	0.0050	0.0094	174.60
4	1	10.65	2.96	6.3611	725.1522	0.0023	0.0030	194.40
	3	11.16	3.11	139.2119	726.6410	0.0024	0.0032	168.00
	4	14.01	3.18	101.4994	772.0008	0.0019	0.0022	173.55
5	1	10.65	3.25	6.3571	725.1483	0.0021	0.0028	168.60
	3	11.16	3.38	139.2064	726.6363	0.0024	0.0030	168.30
	4	14.01	3.46	101.5005	771.9954	0.0039	0.0076	173.40
6	1	10.65	6.18	6.3647	725.1503	0.0021	0.0033	194.40
	3	11.16	6.33	139.2152	726.6379	0.0024	0.0033	168.00
	4	14.01	6.40	101.5034	771.9990	0.0021	0.0026	173.10
7	1	10.65	6.47	6.3621	725.1461	0.0023	0.0034	168.30
	3	11.16	6.60	139.2119	726.6336	0.0025	0.0031	168.00
	4	14.01	6.68	101.5028	771.9938	0.0040	0.0081	173.55
8	1	10.65	7.79	6.3649	725.1502	0.0025	0.0027	194.25
	3	11.16	7.93	139.2160	726.6353	0.0027	0.0041	168.00
	4	14.01	8.01	101.5048	771.9955	0.0020	0.0020	173.10
9	1	10.65	9.40	6.3649	725.1491	0.0026	0.0034	195.30
	3	11.16	9.54	139.2165	726.6365	0.0026	0.0035	168.30
	4	14.01	9.62	101.5081	771.9985	0.0022	0.0024	171.75
10	1	10.65	9.69	6.3630	725.1455	0.0020	0.0025	168.30
	3	11.16	9.82	139.2127	726.6324	0.0024	0.0028	168.15
	4	14.01	9.90	101.5056	771.9894	0.0045	0.0103	176.25

TABLE 7
Thermal Test Solutions

	obs set	scale	rotation (arcsec)	offset (mas) X		Y	
1	1	1.00000 ± 0.00001	2.09 ± 2.75	5.5 ±	0.8	-3.1 ±	0.9
	2	1.00000 0.00001	-0.56 3.02	3.2	0.7	-4.4	0.8
	3	1.00000 0.00001	2.90 2.93	6.2	0.8	-1.1	0.9
	4	1.00000 0.00001	4.32 2.66	0.3	0.7	-3.2	0.8
	5	1.00000 0.00001	-0.89 2.79	3.6	0.7	1.5	0.9
	6	1.00000 0.00001	2.80 2.80	-3.5	0.7	-1.0	0.8
	7	1.00000 0.00001	-0.24 3.01	-1.2	0.8	3.8	1.0
	8	1.00000 0.00001	-2.28 2.68	-4.1	0.7	1.2	0.7
	9	0.99998 0.00001	-1.10 2.88	-5.6	0.7	-0.1	0.8
	10	1.00000 0.00001	-1.71 2.66	-2.3	0.7	4.9	0.9
2	1	1 0	2.09 2.44	5.5	0.7	-3.1	0.8
	2	1 0	-0.58 2.66	3.2	0.6	-4.4	0.7
	3	1 0	2.93 2.60	6.2	0.7	-1.1	0.8
	4	1 0	4.33 2.36	0.3	0.6	-3.2	0.7
	5	1 0	-0.82 2.47	3.5	0.6	1.4	0.8
	6	1 0	2.83 2.48	-3.5	0.6	-0.9	0.7
	7	1 0	-0.16 2.67	-1.3	0.7	3.7	0.9
	8	1 0	-2.34 2.38	-4.1	0.6	1.3	0.7
	9	1 0	-1.26 2.56	-5.7	0.6	-0.2	0.7
	10	1 0	-1.65 2.36	-2.4	0.6	4.8	0.8
3	1	1	0	5.4	0.7	-3.0	0.8
	2	1	0	3.2	0.6	-4.3	0.7
	3	1	0	6.0	0.7	-1.1	0.9
	4	1	0	0.4	0.6	-3.2	0.7
	5	1	0	3.6	0.7	1.3	0.8
	6	1	0	-3.4	0.6	-1.0	0.7
	7	1	0	-1.2	0.7	3.7	0.9
	8	1	0	-4.2	0.6	1.2	0.7
	9	1	0	-5.7	0.6	-0.2	0.7
	10	1	0	-2.3	0.7	4.7	0.8

We shall explore stability within FGS 3 by deriving ordinary astrometric plate solutions and by examining star separations. The guide-star data will be used to assess the inter-FGS stability over this same time period.

6.1 Intra-FGS Stability

We assess the stability of our reference frame over this time span in the presence of the known temperature changes by solving for changes in spacecraft offset, orientation, and FGS scale. Each observation set consists of three stars which form a triangle (each star having position X, Y listed in Table 6). Each observed triangle is compared with an average triangle, i.e., the triangle of average positions for the three stars (Xave, Yave) identified in Fig. 15. We solve for the coefficients in the relationships

$$\text{Xave} = a*X + b*Y + c, \quad (1)$$

$$\text{Yave} = d*X + e*Y + f \quad (2)$$

using standard least-squares techniques. Since solving for six coefficients with three stars produces an exact (degenerate) solution, we cannot produce results for a complete affine transformation. As a consequence, we solve first for four coefficients, which can describe global scale, rotation, and offset changes between the observation sets. The imposed constraints are

$$a = e, \quad b = -d. \quad (3)$$

The results are given as solution 1 in Table 7. To make the table easier to interpret, it displays a dimensonless scale, a rotation in arcsec, α, where

$$\alpha = \arcsin(b) \quad (4)$$

and offsets, c and f, in milliseconds of arc (mas). During the 9.9-h test, the orientation and scale remained constant

within two parts in 10^5. Note that none of the rotations is statistically significant. Even if real, a 2-arcsec rotation translates into a 0.7-mas shift at the extremes of our 150-arcsec wide field.

We then solve for three coefficients, describing only a global rotation and the offsets in each axis. In this case (solution 2 in Table 7) we have the constraints

$$a=e, \quad b=-d, \quad \text{and} \quad a^2+b^2=1. \tag{5}$$

Again, the rotations are statistically insignificant.

Since rotation and scale changes are extremely small, we finally solve for two coefficients only, the offsets in X and Y (solution 3 in Table 7), by constraining

$$a=e=1, \quad b=-d=0. \tag{6}$$

The only obvious trend in the offsets is the abrupt shift in c, between observation sets 5 and 6. This is seen in each solution, is an artifact due to reacquisition of the guide stars between the sets, and is inconsequential. Table 6 indicates that such reacquisitions took place between sets 1 and 2, 3 and 4, 5 and 6, 7 and 8, and 8 and 9. Rather remarkably, the shifts between most of the guide star reacquisitions are quite small. Most offset changes are <3 mas.

From Table 7 we conclude that there were no scale or rotation changes over 9.9 h, to well within the precision of the measurements. The reference frame is internally consistent at the 0.001-arcsec level.

As another check of the short-term thermal stability, we calculated the radial separations between the star pairs 1–3, 1–4, and 3–4 for each of the sets listed in Table 6. We then calculated the difference between these separations and the average separation determined from all sets. These separations (which reflect changes from the average, only) and associated standard deviations are plotted in Fig. 17. The changes in separation with time are in no case statistically significant and so confirm the scale results above.

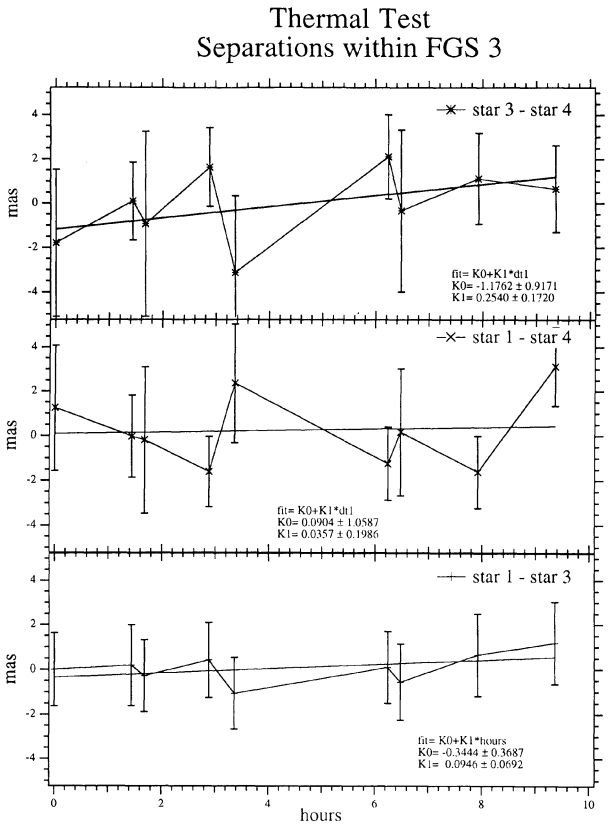

FIG. 17—We plot the normalized radial separations (in milliarcsec) of stars 3 and 4 (top), stars 1 and 4 (middle), and stars 1 and 3 bottom against elapsed time in hours after the start of the thermal test. The trend lines are unweighted fits to the individual data points. We see no statistically significant trends in these data.

6.2 Inter-FGS Stability

The stability of the entire *HST* Optical Telescope Assembly can be assessed by considering the temporal variations in the separations between the guide stars used for the thermal test. These guide stars are identified in Fig. 15. Remembering that the Y direction in FGS 1 corresponds to the X direction in FGS 2, we derive the separations along the X and Y axes.

We present the raw separations for each two guide-star fine-lock event during the test in Fig. 18. The crosses are the raw separations uncorrected for velocity aberration caused by the *HST* orbital motion. The squares are the raw separations after correction for *HST* velocity aberration, using velocity information from the definitive orbit. Note the repeated structure within each orbit. We may be detecting real *HST* structural changes.

Since no spacecraft or FGS temperatures are varying on the 0.03-day time scale of the intraorbit guide-star separation changes shown in Fig. 18, we, for now, ignore this structure. To reduce the noise, the X and Y values for all the guide-star separations within each orbit listed in Table 6 were averaged. The difference from the average separation over the entire test is calculated and plotted in Fig. 19. Thus, the separations plotted in Fig. 19 are the result of an average of from five to six positions.

In the X direction of FGS 1 (which is also the X direction in FGS 3) we see no statistically significant separation variation. However, in the Y direction of FGS 1 (also the $-Y$ direction in FGS 3) we see a statistically significant change over the 10 h test. Expressed as a scale change, the variation along the Y direction in FGS 1 and FGS 3 represents 3 parts in 10^6, interesting that it can be seen at all, but probably not astrometrically offensive. Finally, we plot (Fig. 20) the change in the average radial separation during the test. Within the errors, there is no change. The straight-line fit has a slope $=0.17\pm0.12$ ms of arc h^{-1}. This translates to a change of one part in 10^6 over the entire test duration for this particular separation.

Since a normal *HST* astrometry observation requires on the order of 1 h, no changes detected during this typical orientation will have any impact. However, in 1992 we plan to carry out a test which will provide a more extreme thermal disturbance to FGS 2 and assess the effects of this on POS-mode astrometry.

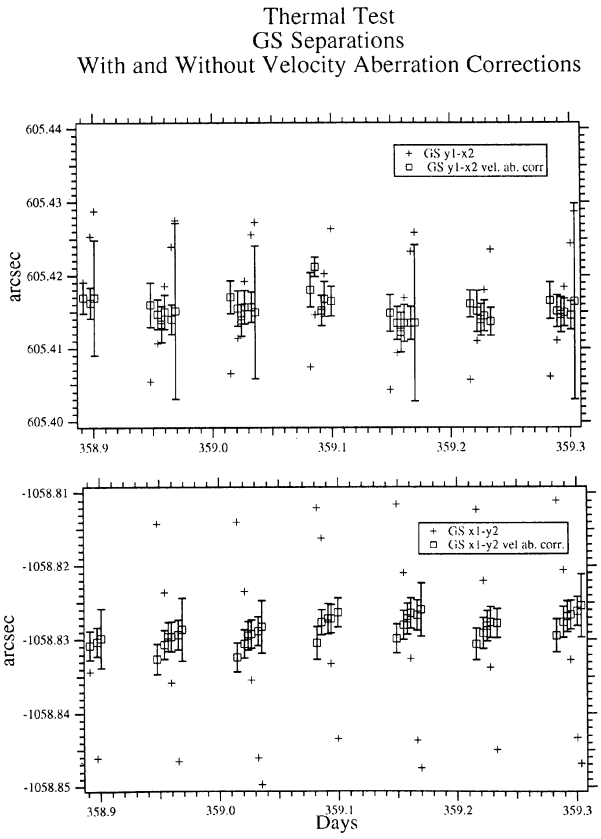

FIG. 18—The raw (+) and spacecraft-velocity aberration corrected (□) $Y1-X2$ (top) and $X1-Y2$ (bottom) guide-star separations (in milliarcsec) are plotted against time (day of year 1991). GS $y1-x2$ is the separation between the guide stars derived from the Y component of FGS 1 and the X component of FGS 2. GS $x1-y2$ is the separation between the guide stars derived from the X component of FGS 1 and the Y component of FGS 2. The velocity aberration corrections were made using the predicted *HST* orbit. The trends within each group of velocity aberration corrected separations may be significant.

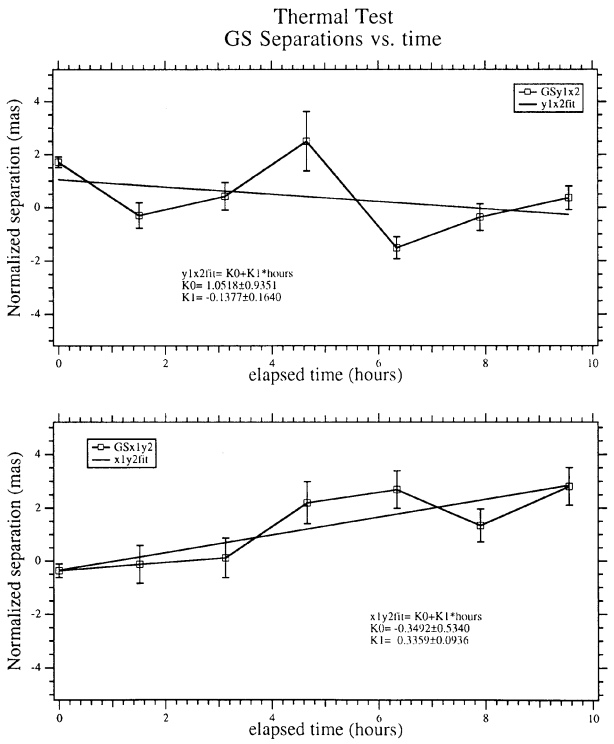

FIG. 19—Normal points from Fig. 18 are subtracted from the average x and y GS separation and plotted against elapsed time in hours after the beginning of the thermal test.

7. DISCUSSION AND CONCLUSIONS

Of the nine Astrometry Verification target stars listed in Table 1, three have cluster membership probabilities >98% (van Altena et al. 1992). For two of these stars (Upgren-108 and -111), we have successful fine-lock POS-mode observations from FGS 3. These observations provide a lower limit on duplicity. For two stars of equal magnitude, we could not achieve fine lock for separations >0.03 arcsec.

Can we determine a pickle-wide POS-mode limiting magnitude for FGS 3? Yes, if we are convinced that better S curves imply better POS-mode performance. We have faint star observations only in the center of FGS 1 and 3. However, the poorest S curve in FGS 3 [at the edges of the pickle, both sides of Fig. 5(a)] is about the same quality as that anywhere in FGS 1 [Fig. 3(a)]. We obtained a successful POS-mode observation of the $V=16$ star with full aperture F583W in FGS 1 at pickle center (Sec. 4.2.1). With no variations in S curves across the pickle [Fig. 3(a)], this success could have occurred anywhere in FGS 1. As we have seen in Sec. 2, the limiting magnitude in FGS 3 is about 0.3 mag fainter than that in FGS 1, because of the more sensitive PMTs in FGS 3. So, we conclude that the POS mode limiting magnitude in FGS 3 at the pickle extremes, where the S curves are poorest, must be about 16.3 with the F583W filter.

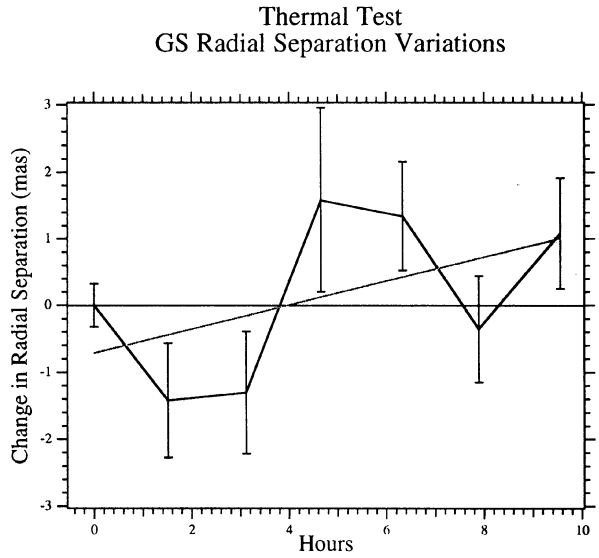

FIG. 20—Changes in GS radial separation during the thermal test. The fit relationship has only marginal statistical significance and amounts to one part in 10^7 per hour.

Pushing this argument a little further, we can predict an FGS 3 POS-mode limiting magnitude for the region containing the central three filled-in circles of Fig. 6. From Fig. 5(a) we see these locations have similar quality S curves. They will likely have similar POS mode capability. We successfully observed $V=17.02$ in the central of these three locations (Sec. 4.1.2). Hence, we predict a $V=17$ limit for the other two locations. Thus, fully half of FGS 3 may have our originally sought magnitude limit. Finally, with the PUPIL the POS-mode performance of this central region of FGS 3 should be about $V=16.2$, since we lose about 0.77 mag sensitivity compared to F583W (Table 3).

In 1991 December *HST* was not a stable platform from which to carry out 0.003-arcsec precision astrometry. In the period 24–29 December we attempted 95 POS and TRANS mode observations for Orbital Verification. Of these, 32 were adversely affected by jitter. Either the shaking was of high enough amplitude to kick the guiding FGS out of fine lock, or, even though fine lock was held, the astrometry FGS was not held stable, increasing the observational errors to an unacceptable level. The almost always higher Y axis standard deviations (compared to those for the X axis) argue that nearly all these data are to some degree tainted by *HST* jitter.

A new servo control law was placed on board *HST* in 1991 April. Preliminary results suggest that the response of the guiding FGS to terminator disturbances has been improved. Loss of lock may be occurring less frequently. This is a temporary and not totally satisfactory fix. The solar arrays still flex with each sunrise and sunset. The vehicle continues to be disturbed. The upcoming servicing mission to replace the solar arrays is essential to obtain the very best astrometry that *HST* is capable of providing.

We will demonstrate a full astrometry capability for *HST* with a series of Science Verification tests, either in progress or to occur later this year. These include a long-term geometric stability test, a complete determination of the FGS 3 optical field angle distortions, and a lateral color test. The first test will indicate whether or not changes in the focal plane or FGS structures occur over time scales of months. The second will allow us to map, and thus remove, the optical distortions in FGS 3 (Benedict et al. 1991). The last test will determine position shifts as a function of star color, due to the refractive elements in the FGS (Bradley et al. 1991).

In conclusion, from on-orbit performance FGS 3 has been demonstrated to have better astrometric qualities than FGS 1, prompting the Astrometry Science Team to choose FGS 3 to be the prime astrometer. Specifically, FGS 3 has been shown to produce POS mode measurements on a star with $V=17$ with a per-axis precision of 0.003 arcsec. TRANS mode appears to be a viable technique at least down to $V=16$. S-curve characteristics render FGS 3 less sensitive to loss of lock in the presence of jitter. In a 10-h test of the stability of astrometric measurements, we found no scale or orientation variations within FGS 3 greater than two parts in 10^5. During this same time period, we found no significant guide star radial separation changes.

The Astrometry Science Team is supported by NASA Grant No. NAG5-1603. We would like to thank the many Space Telescope Science Institute support staff who aided us in the proposal process, particularly Lauretta Nagel. These data would not have been secured without the essential support of many at the Goddard Spaceflight Center *HST* Operations Center.

REFERENCES

Benedict, G. F., and Shelus, P. J. 1978, in Proc. IAU, Colloq. No. 48, Modern Astrometry, ed. F. Prochazka and R. Turner (Vienna, University Observatory)

Benedict, G. F. et al. 1991, in The First Year of *HST* Observations, ed. A. L. Kinney and J. C. Blades (Baltimore, Space Telescope Science Institute)

Bradley, A., Abramowicz-Reed, L., Story, D., Benedict, G., and Jefferys, W. 1991, PASP, 103, 317

Burrows, C. J., Holtzman, J. A., Faber, S. M., Bely, P. Y., Hasan, H., Lynds, C. R., and Schroeder, D. 1991, ApJ, 369, L21

Franz, O. G. et al. 1991, ApJ, 377, L17

Jefferys, W. H., Benedict, G. F., Hemenway, P. D., Shelus, P. J., and Duncombe, R. L. 1985, Celest. Mech., 37, 299

Lasker, B., Sturch, C., McLean, B., Russell, J., Jenkner, H., and Shara, M. 1990, AJ, 99, 2019

McCartney, J., Jefferys, W., and McArthur, B. 1990, BAAS, 22, 932

Sandage, A. R. 1962, ApJ, 135, 333

Taff, L. G. 1990, *Hubble Space Telescope* Fine Guidance Sensors Instrument Handbook, Version 2.1 (Baltimore, Space Telescope Science Institute)

Upgren, A. R., Mesrobian, W. S., and Kerridge, S. J. 1972, AJ, 77, 74

van Altena, W., Yang, T., and Girard, T. 1992, private communication